BioNanoScience (2025) 15:153
https://doi.org/10.1007/s12668-024-01675-8

RESEARCH

Development of Water-Soluble Nanoformulations of Novel Pyrazolone Derivatives and the Evaluation of Their Antibacterial and Antioxidant Activities

Nkeiruka N. Igbokwe[1,5] · Eman A. Ismail[1,6] · Vincent A. Obakachi[2] · Aviwe Ntsethe[3] · Mlindeli Gamede[4] · Rajshekhar Karpoormath[2] · Mbuso A. Faya[1]

Accepted: 6 October 2024

Abstract

Poor aqueous solubility and stability hinder the clinical translation of pyrazolone-based derivatives despite their various biological activities. This study aimed to address these issues by developing water-soluble nanoformulations of two specific pyrazolone derivatives, Compounds I and II, selected based on their promising structural features and previous biological activity data. PLGA/poloxamer-based nanoformulations were prepared and optimized for size, PDI, zeta potential (ZP), and entrapment efficiency (EE). The optimized formulations demonstrated sizes of 166.6 ± 7.12 nm and 192.5 ± 1.08 nm, PDI of 0.129 ± 0.042 and 0.132 ± 0.025, ZP of -14.14 ± 2.90 mV and -10.77 ± 1.515 mV, and %EE of 84.20 ± 0.930 and 81.5 ± 2.051, respectively. A sustained drug release was observed over 48 h, with cumulative releases of approximately 37% and 53%, for both formulations, and characterized by a complex drug release behavior. The formulations exhibited significant antibacterial activity against Methicillin-resistant *Staphylococcus aureus* (MRSA) and *S. aureus* (SA), with greater than 90% cell death for SA and greater than 80% for MRSA, observed using the flow cytometer. Also, enhanced antioxidant activity was observed using DPPH, FRAP, and NO methods, showing better radical scavenging than standard gallic acid and bare compounds. The hemolysis assay confirmed the biocompatibility of the developed formulation, with a hemolysis percentage of less than 5%. This study highlights the successful development of water-soluble nanoformulations with significant antibacterial and antioxidant activities, emphasizing the impact of solubility enhancement on biological efficacy and suggesting potential pharmaceutical applications for these agents.

✉ Mbuso A. Faya
FayaA@ukzn.ac.za

1 Department of Pharmaceutics, Discipline of Pharmaceutical Sciences, College of Health Sciences, University of KwaZulu-Natal, Durban 4000, South Africa

2 Department of Pharmaceutical Chemistry, Discipline of Pharmaceutical Sciences, College of Health Sciences, University of KwaZulu-Natal, Durban 4000, South Africa

3 School of Laboratory Medicine and Medical Sciences, College of Health Sciences, University of KwaZulu-Natal, Durban 4000, South Africa

4 Department of Physiology, School of Medicine, Faculty of Health Sciences, University of Pretoria, Pretoria, South Africa

5 Department of Pharmaceutics and Pharmaceutical Technology, Faculty of Pharmacy, University of Maiduguri, Maiduguri, Borno State, Nigeria

6 Department of Pharmaceutics, Faculty of Pharmacy, University of Gezira, Wad Medani, Sudan

Published online: 26 December 2024

Graphical Abstract

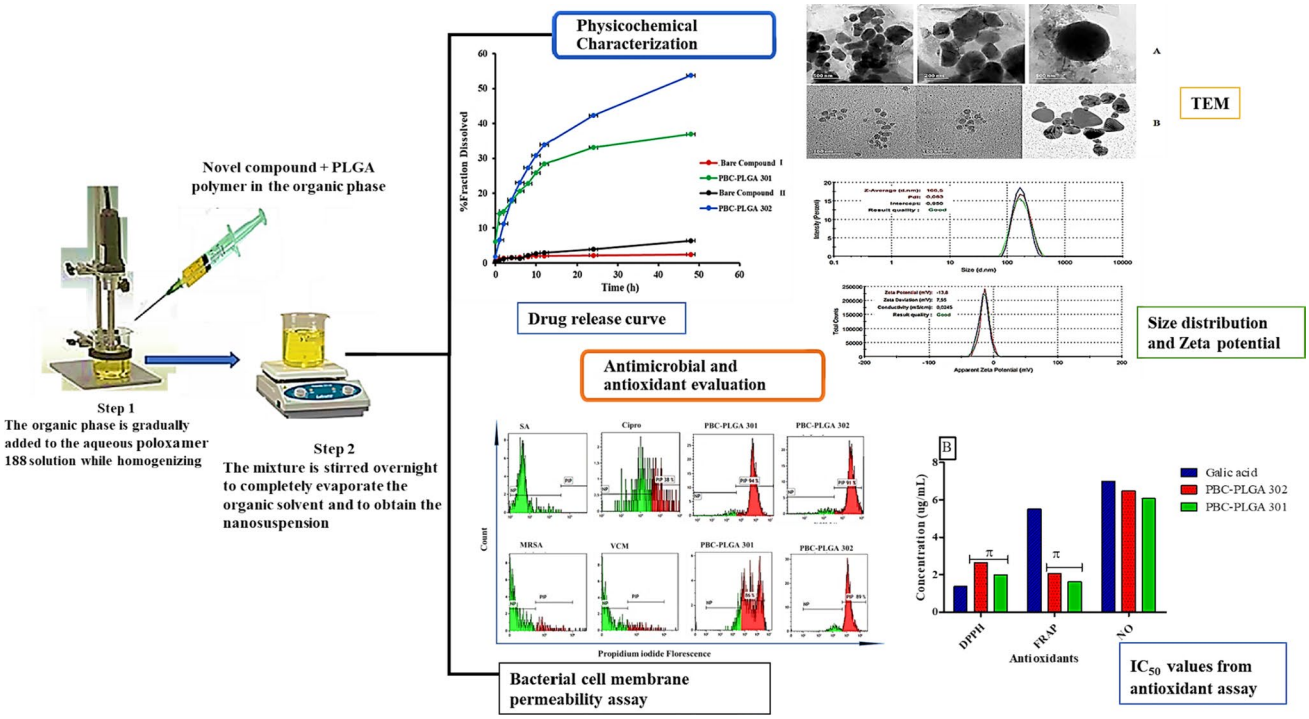

Keywords Pyrazolone derivatives · Solubility enhancement · Antioxidant · Flow cytometry · Antibacterial · Nanoformulation

1 Introduction

Poor aqueous solubility of new drug candidates can make it difficult to produce efficient therapeutic formulations and impede in vitro investigations and in vivo toxicity assessments [1, 2]. Moreover, drug solubility is a significant predictor of dissolution rate, and inadequate solubility can lead to reduced bioavailability of oral drugs, poor clinical outcomes, and therapeutic failure [3]. Solubility evaluation is, therefore, a crucial step in developing new drugs, especially when developing dosage forms and choosing which ones to use in clinical trials, planning experiments, developing analytical methods, and developing drug manufacturing strategies. Consequently, designing formulations that make medicines more soluble can increase their bioavailability and effectiveness [4].

Along with several other traditional methods, nanoformulation is thought to be the most convenient way to increase water solubility. It has been observed that adding loaded substances to suitable nanoparticles (NP) in the size range of 10–1000 nm improves their solubility and bioavailability [5–7]. Polymer-based nanosystems are the most often utilized for this purpose because they are simple to prepare, stable over time, have fewer toxic effects, and can effectively encapsulate hydrophobic medicines [7, 8]. To this effect, a wide range of polymers and copolymers, including chitosan, alginate, gelatin, poly(lactic-co-glycolic acid) (PLGA), polylactic acid (PLA), poly(caprolactone) (PCL), and polyglycolide, have been thoroughly reviewed [9, 10]. However, PLGA is the most widely used [11].

PLGA is a synthetic polymer with appealing qualities, including biodegradability and biocompatibility, drug targeting, the capacity to protect loaded drugs from chemical instability, and the potential for better interaction with biological materials through improved surface properties [12, 13]. PLGA is recognized as safe for parenteral administration by the EMA (European Medicine Agency) and US FDA (United States Food and Drug Administration) [14–16]. Moreover, data suggested that PLGA polymeric nanoparticles were used to improve the solubility of several natural and synthesized bioactive chemicals, including quercetin, curcumin, resveratrol, and brucine [17–20]. All these properties inspired the use of PLGA as a choice polymer in this study.

Pyrazolones are pyrazole derivatives with an extra carbonyl (C = O) group having a five-membered lactam ring structure with two nitrogen and one ketonic group.

Owing to the planar structure of the aromatic heterocycle, the pyrazole nucleus exhibits practically all forms of pharmacological actions and has caught the interest of many researchers over the years, making it one of the most researched pharmacophores in the world. They are a key component of medicines and synthetic products with analgesic, antioxidant, antimicrobial, antifungal, anti-inflammatory, anti-tumor/anti-cancer, gastric secretion stimulatory, antidepressant, antidiabetic, antiviral, and anthelmintic properties [21–26].

The novel pyrazolone derivatives described in this work were previously designed, synthesized, and characterized in our laboratory as poorly soluble. The results for the synthesis methods and characterization of 2-(2-((2E,3E)−4-(5-ethoxy-3-methyl-1-phenyl-1l4,2l2-pyrazol-4-yl)but-3-en-2-ylidene)hydrazinyl)−4-(4-fluorophenyl)thiazole (Compound I) and (E)−2-((E)−4-(5-ethoxy-3-methyl-1-phenyl-1H-pyrazol-4-yl) but-3-en-2-ylidene)hydrazine-1-carbothioamide (Compound II) have been reported by Obakachi et al. Both compounds have previously been screened for activities against the SARS-CoV-2 virus and cancer cell lines in silico [27, 28]. However, poor water solubility hindered further research into the in vitro and in vivo biological activities of these compounds and, as a result, their potential for pharmaceutical use.

Hence, this research explored the development of a water-soluble formulation of Compounds I and II using PLGA with poloxamer complexes. Also, to assess the antibacterial and antioxidant activities of the compounds while determining the impact of solubility enhancement on their in vitro performance, the prepared nanoformulations were efficiently characterized for optimum physicochemical properties and were screened for antioxidant and antibacterial activities. Antioxidant testing was conducted to establish the percentage of radical scavenging activity using 2,2-diphenyl-1-picrylhydrazyl (DPPH), nitric oxide (NO), and ferric-reducing antioxidant power (FRAP) methods. Also, antibacterial activity testing using the minimum inhibitory concentration (MIC) method and cell penetration experiments to quantify the extent of bacterial kill using the flow cytometer were performed.

2 Materials and Methods

The new compounds were previously synthesized, chemically characterized, and reported by Obakachi et al. [27], and the chemical structures are depicted in Fig. 1. Materials used are Poly (lactic-co-glycolic acid) (PLGA) 50:50, poloxamer-188 (Sigma-Aldrich), phosphate-buffered saline (PBS) tablets (Sigma-Aldrich), sodium lauryl sulfate, methanol (HPLC grade), and acetone (HPLC grade). Others included Iodonitrotetrazolium chloride (INT), dimethyl sulfoxide (DMSO), propidium iodide (Biocom Africa), ciprofloxacin (Sigma-Aldrich, St-Quentin-Fallavier, France), Mueller–Hinton agar, Mueller–Hinton broth (Sigma-Aldrich) and were all of the analytical grades. While organic reagents were utilized without additional purification, all aqueous solvents were purified according to standard protocols.

2.1 Preparation of PBC-PLGA Nanoparticles

The nanoformulations were prepared using the nanoprecipitation technique with slight modifications [29]. In a nutshell, 60 mg of PLGA, 1% poloxamer, and 6 mg of the bare compounds were weighed. The 60 mg PLGA was dissolved in 5 mL of acetone, and the compound was dissolved in 500 µL of suitable organic solvent, mixed with the PLGA solution while stirring, and then added in drops to 10 mL poloxamer solution while homogenizing for 5 min at 30% power. The setup was stirred at 600 rpm overnight to evaporate the organic solvent completely to obtain the PBC-PLGA nanosuspension. A blank sample without the compounds was also prepared in this manner. Each sample was made in triplicate and appropriately labeled as PBC-PLGA 301 and PBC-PLGA 302 for Compounds I and II, respectively.

2.2 Physicochemical Characterization of PBC-PLGA Nanoparticles

2.2.1 Identification and Quantification of the Pyrazolone-Based Compounds

The pyrazolone molecules were identified and quantified using a Shimadzu HPLC system (Kyoto, Japan) outfitted with binary high/low-pressure gradient pumps, a degasser,

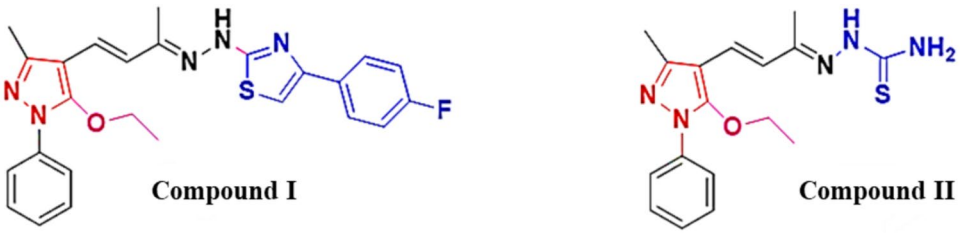

Fig. 1 Structure of the novel compounds

a PDA detector, and an autosampler using LC Solution 5.106 SPI system software. Shim-pack GIST C18 (5 µm, 150 cm, 4.6 mm) column was used for efficient separation and quantification at 25 °C with isocratic elution using acetonitrile and acidified water (0.1% trifluoroacetic acid) with 20 µL injection volume. The mobile phase ratios were 85:15 and 75:25, with flow rates of 1 mL/min and 0.5 mL/min at wavelengths of 203 nm and 333 nm, respectively, for Compounds I and II. The calibration curve regression equations for the compounds were $Y = 65356X - 24{,}472$ and $Y = 274470X - 94{,}958$, with linearity correlation coefficients R^2 of 0.999 and 0.9994, respectively. Additional data for method validation are provided in the supplementary material section of this article.

2.2.2 Determination of the Particle Size, PDI, and Surface Charge of the Formed PBC-PLGA Nanoparticles

Dynamic light scattering (DLS) was deployed to evaluate the size, PDI, and ZP of the prepared nanoparticle suspensions at 25 °C using a zeta sizer (Nano ZS, Malvern Instruments, UK). The samples were diluted with Milli-Q water until the scattering intensity was within the sensitivity range of the instrument, and then they were analyzed. The three measured averages and standard deviations were provided.

2.2.3 Determination of Entrapment Efficiency and Drug-Loading Capacity

The nanoparticles were collected by centrifugation at 12,000 rpm for 30 min at 4 °C. High-performance liquid chromatography (HPLC–PDA) was used to estimate the entrapment efficiency by measuring the amount of free drug in the supernatant [30]. One milliliter of methanol/acetone was added to 500 µL of nanosuspension, sonicated for 15 min and made up to a volume of 10 mL in a volumetric flask, filtered, and analyzed as previously described, to determine the drug content concentration. The experiment was carried out in triplicate. Equations 1 and 2 were used to calculate the drug content and entrapment efficiency.

$$\text{Loading capacity} = \left(\frac{\text{mg}}{\text{mL}}\right)\frac{\text{Amount of the drug in a nanosuspension} - \text{unentrapped}}{\text{The total weight of the nanoparticles}} \times 100 \quad (1)$$

$$\text{Entrapment efficiency} = \frac{\text{Amount of drug in nanosuspension} - \text{unentrapped}}{\text{Amt of the drug in nanosuspension}} \times 100 \quad (2)$$

2.2.4 Differential Scanning Calorimetry (DSC)

DSC (Shimadzu DSC-60, Japan) was used to investigate the thermal profiles of the bare Compounds I and II, P188, PLGA, physical mixture of the formulation components, and lyophilized PBC-PLGA nanoparticles. In brief, samples (2 mg) were put in an aluminum pan and sealed with a crimper before being heated to 300 °C at a constant rate of 10 °C per minute under a continuous nitrogen flow of 20 mL/min using an empty pan as a reference.

2.2.5 Transmission Electron Microscope

Transmission electron microscopy (JEOL, JEM-1010 (Japan)) was used for the morphological studies (TEM). The PBC-PLGA nanosuspensions were properly diluted before being put on the surface of a copper grid. Before measuring, the surplus material was blotted out using filter paper, which was then dried at room temperature and dyed with a 2% uranyl acetate solution [31]. All images were taken at an accelerating voltage of 100 kV.

2.2.6 Scanning Electron Microscope (SEM)

The light electron microscope (SDP TOP, CX 40, Ningbo Sunny Instruments Co., Ltd) and the field emission scanning electron microscope (FESEM, JEOL JSM-6700) were used to examine the surface morphology and solid-state characteristics of the PLGA-PBC nanoparticles. The nanoparticle dispersion was deposited onto the copper tape and air-dried before being sputtered by gold for 120 s and visualized at a voltage of 5 kV and a current of 10 A. The (ImageJ 32) image processing tool was used to create the SEM micrographs.

2.2.7 In Vitro Drug Release Studies

In vitro release studies of the pyrazolone-based compounds from PLGA nanoparticles were carried out at 37 °C by dialysis bag diffusion technique. Briefly, 2.0 mL of the suspended nanoparticulate dispersion was placed in a pre-hydrated cellulose dialysis bag (cutoff 10,000 Da, Sigma-Aldrich) and immersed in a 20.0 mL of pH 7.4 phosphate buffer solution

and 0.3% sodium lauryl sulfate (SLS) in the receptacle compartment (50 mL falcon tube) and incubated in a shaking incubator at 100 rpm. SLS was employed in the PBS not only to maintain sink condition but also to provide solubility for the bare compounds in the aqueous phase. Two milliliter samples from the recipient compartment were withdrawn at pre-set time intervals of 0, 2, 4, 6, 8, 10, 12, 24, and 72 h and replaced with the fresh release medium of the same volume. The PBC content in the release samples was determined using the previously described HPLC–PDA method. All experiments were set up in triplicate, and the average values were calculated. The results were analyzed using Excel add-in DDsolver, and the release profiles are presented in the "Results and Discussions" section of this article. The cumulative release data were further fitted with different drug release kinetic equations to analyze the drug release behavior.

2.2.8 Stability Study

A stability study was performed for the optimized formulations to determine the best storage condition and shelf life of the prepared formulation. The PBC-PLGA NPs were investigated for particle size, PDI, and zeta potential at 4 °C and 25 °C for 0, 7, 30, 60, and 90 days, respectively. All experiments were set up in triplicate, and the average values were calculated.

2.3 Evaluation of the Antibacterial Activity

2.3.1 Determination of Bacterial Susceptibility

INT colorimetric assay was conducted in clear, sterile 96-well microtiter plates (Corning Life Sciences, Acton, MA, USA) [32] to assess the minimal inhibitory concentrations (MICs) of the pyrazolone derivatives (Compounds I and II) and their nanoformulations (PBC-PLGA 301 and PBC-PLGA 302). Vancomycin and ciprofloxacin were used as standards against two gram-negative bacteria, viz, *Pseudomonas aeruginosa* (PA) ATCC 27853 and *Escherichia coli* (EC) ATCC 25922, and two gram-positive bacteria, viz, *Staphylococcus aureus* (SA) ATCC 25923 and *Methicillin-resistant staphylococcus aureus* (MRSA) ATCC 10069. Ciprofloxacin was used as drug control for PA, EC, and SA, whereas vancomycin was used for MRSA. Viable bacteria reduced the colorless dye to pink. The minimum inhibitory concentration was the lowest sample concentration, which prevented this change after incubation and exhibited complete inhibition of microbial growth.

2.3.2 Cell Membrane Penetration Assay Using Flow Cytometry

Flow cytometry evaluated the ability of the nanoformulations PBC-PLGA 301 and PBC-PLGA 302 to penetrate MRSA and SA membranes. Briefly, MRSA and SA cells prepared according to the bacterial susceptibility protocol earlier described were harvested after 24 h of incubation and incubated with propidium iodide dye (PI) (5 µL) for 30 min at room temperature. Fifty microliters of each sample mixture was transferred into sample vials, with each tube containing 350 µL of the sheath fluid and vortexed for 1 min. The cell-penetrating efficiency of the samples was then investigated by FACScan analysis via the influx of PI into the bacterial cells. The PI fluorescence was excited by a 488 nm laser and collected through a 617-nm bandpass filter (red wavelength). The untreated MRSA cells were the negative control. The CytoFLEX (Beckman Coulter Life Sciences, USA) equipment was used for flow cytometry. Instrumentation settings included a sheath fluid flow rate of 16 mL/min and a sample flow rate of 30 µL/min. The voltage settings used for fluorescence-activated cell sorting (FACS) analysis were 731 (forward scatter FSC), 538 (side scatter SSC), and 444 for PI [33]. The bacteria were initially gated using forward scatter, and cells of the appropriate size were then gated, and at least 10,000 cells were collected for each sample in triplicate. Moreover, the detection threshold was set at 1000 in SSC analysis to avoid any background signals from particles smaller than the bacteria. Data with fixed cells were collated and analyzed using the flow cytometer software Kaluza 2.1 (Beckman Coulter USA).

2.4 In Vitro Hemolysis Study

A previously described method was used to determine the percentage of hemolysis [33]. Briefly, freshly collected sheep blood was washed three times with autoclaved phosphate-buffer saline (PBS, pH 7.4) centrifuged at 3500 rpm for 15 min. Blank formulation and PBC-PLGA (301 and 302) were diluted with PBS to make concentrations ranging from 0.05 to 0.5 mg/mL for each sample. The RBC suspension (0.2 mL) was added to 1.8 mL of each sample and incubated at 37 °C for 30 min. After which, the samples were centrifuged at 3000 rpm for 10 min, and spectrophotometric readings of the supernatant of each sample at different concentrations were taken at 416 nm wavelength to determine hemoglobin release. To obtain 0% and 100% hemolysis, 0.2 mL of RBC suspension was added to 1.8 mL PBS and distilled water. The degree of hemolysis was calculated using the equation below:

$$Hemolysis(\%) = \frac{(Abs - Abs0)}{(Abs100 - Abs0)} \times 100 \quad (3)$$

Abs100 and Abs0 are the absorbances of the solution at 100% and 0% hemolysis, respectively.

2.5 Radical Scavenging Activity of the Bare Novel Compounds and PBC-PLGA Nanoparticles

2.5.1 DPPH (2,2-Diphenyl-1-Picrylhydrazyl) Scavenging Activity

One hundred microliters of each sample at different concentrations of 3.5, 7.5, 15, 30, and 60 µg/mL for the nanoformulations and 15, 30, 60, 120, and 240 µg/mL for the free compounds was incubated with 50 µL of 0.3 mM DPPH solution (in methanol) and placed in the dark for 30 min at ambient temperature. The absorbance was then read at 517 nm against a blank sample of DPPH solution.

The scavenging ability was calculated using the equation below:

$$\text{DPPH radical scavenging} = \frac{Ac - As}{Ac} \times 100 \quad (4)$$

Ac represents the absorbance of the control, and As represents the absorbance of the sample.

2.5.2 FRAP (Ferric-Reducing Antioxidant Power)

The total ferric-reducing power of the compounds (I and II) and PBC-PLGA nanoparticles was measured using the FRAP method described by Oyaizu [34] with slight modifications. Briefly, 1 mL of each test sample (concentrations 3.5–60 µg/mL and 15–240 µg/mL) for the PBC-PLGA nanosuspension and bare Compounds I and II, respectively, was incubated with 1 mL of sodium phosphate buffer (0.2 M, pH 6.6) and 1% potassium ferricyanide at 50 °C for 30 min. After that, 1 mL of 10% trichloroacetic acid was used to acidify the reaction mixtures. Then, 1 mL of the sample was mixed with an equal volume of distilled water and 200 µL of 0.1% $FeCl_3$. The absorbance of the resultant solution was read at 700 nm in a spectrophotometer. Antioxidant activity was calculated using the equation below:

$$\%\ \text{FRAP radical scavenging} = \frac{\text{Absorbance of control} - \text{absorbance of the test sample}}{\text{Absorbance of control}} \times 100 \quad (5)$$

2.5.3 Nitric Oxide (NO) Radical Inhibitory Activity

At physiological pH, sodium nitroprusside could create much nitric oxide (NO), reacting with oxygen to form nitrite ions. This capability forms the basis of this test [35]. The test was performed by incubating 500 µL of 10 mM sodium nitroprusside in sodium phosphate buffer (pH 7.4) and 500 µL of the test samples at various concentrations (15–240 µg/mL) for 2 h at 37 °C. The reaction mixture was then given a 500 µL dose of Griess reagent. The absorbance was measured at 546 nm to detect a chromophore formed by the reaction of nitrite with sulfanilamide. By comparing the absorbance of a prepared control to the percentage inhibition of NO release, the percentage inhibition of NO emitted was computed (10 mM sodium nitroprusside in phosphate buffer). The experiment was performed in triplicates, and the test sample's scavenging capacity was calculated using the formula below:

$$\%\ \text{scavenging activity} = \frac{\text{The absorbance of control} - \text{Absorbance of test Sample}}{\text{absorbance of control}} \times 100 \quad (6)$$

2.6 Data Analysis

Experimental data were presented as mean ± standard deviation (SD) and analyzed using the Excel Analysis toolkit. The one-way ANOVA defined statistical significance as a p-value of < 0.05.

3 Results and Discussions

The low solubility of these newly synthesized, pyrazolone-based compounds restricts their pharmaceutical and clinical translation. However, we tried to create efficient PBC-encapsulated PLGA nanoformulations to address this solubility problem in light of the various therapeutic uses of the pyrazolone nucleus. We further characterized these PBC-PLGA nanoformulations and performed in vitro antibacterial and antioxidant activity tests and cell penetration assay using the flow cytometer to determine the impact of solubility enhancement on the compounds.

3.1 Preparation of PBC-PLGA Nanoparticles

An effective method for encapsulating hydrophobic substances involves selecting the appropriate polymer composition, stabilizer, solvent-drug solubility, and manufacturing method [36]. Formulating the selected compounds into nanoparticles was highly required to solubilize them. Based on its solid-state solubility and biocompatibility, poly(lactic-co-glycolic acid) polymer (PLGA) was employed to encapsulate the pyrazolone-based molecules effectively [37–39]. The nanoprecipitation technique mentioned in the procedure

section generated the PBC-PLGA nanoparticles. The spontaneous diffusion between the organic and aqueous phases propels the production of the nanoparticles in this situation. Due to programmable formulation parameters, this technology is an example of a bottom-up approach that permits the production of particles with the appropriate qualities [40, 41].

Expressive, the physical characteristics such as solubility, thermal strength, viscosity, crystallinity, mechanical strength, and degradation rate depend on the polymer's molecular weight [42, 43]. As a result, a low molecular weight 50/50 PLGA was used as the carrier for the compounds. We paid close attention to the solvent selection since it impacts the drug entrapment level, polydispersity, and nanoparticle size. Therefore, acetone was chosen as the organic solvent for this study. The sonication intensity, duration, and stirring rate were varied to optimize the nanoparticle formulation. Furthermore, the impact of several surfactants, polyvinyl alcohol, poloxamer-188, and span 80, on the physicochemical characteristics of the nanoparticles, was evaluated to choose an appropriate stabilizer that could successfully assure the stability of nanoparticles. With a sonication time of 5 min at 30% power, a stirring speed of 600 rpm, and 1% poloxamer-188 as the stabilizer, the ideal size, PDI, and zeta potential were obtained.

3.2 Size, PDI, Zeta Potential, and Surface Morphology of Nanoparticles of PBC-PLGA

The physicochemical properties of the generated PBC-PLGA nanoparticles are shown in Table 1, distribution curves for size and zeta potential are shown in Figs. 2 and 3, and SEM and TEM surface morphology diagrams are in Figs. 4 and 5.

Particle size is recognized to be an important component in particle cellular absorption and intracellular trafficking, making tiny particles more efficient than their micron-sized counterparts in medication delivery to infected loci [30]. Particles with sizes ranging from 100 to 200 nm are appropriate for long-term circulation and facile transfer across biological membranes. In contrast, nanoparticles larger than 200 nm are phagocytosed and mostly transported to the liver and spleen [44]. The nanoparticle suspensions had monodispersed size distributions (PDI < 0.15), with an intensity-averaged diameter measured by DLS of < 200 nm the PBC-PLGA nanoparticles (Z-Ave = 166.6 ± 7.12 nm and 192.5 ± 1.08 nm). As a result, they are appropriate for parenteral administration, with facile penetration through membranes, focused distribution, and maintained circulation. Even though the sizes obtained in this study appeared to be more significant than those reported by Alfei and Sun et al.

Table 1 Optimized size, PDI, zeta potential, entrapment efficiency, and drug-loading capacity of the PBC-PLGA nanoformulations

Sample	Size (nm)	PDI	Zeta potential (mV)	Entrapment efficiency (%)	Drug-loading capacity (%)
PBC-PLGA 301 NPs	166.6 ± 7.12	0.129 ± 0.042	− 14.14 ± 2.900	84.20 ± 0.930	0.30 ± 0.000
PBC-PLGA 302 NPs	192.5 ± 1.08	0.132 ± 0.025	− 10.77 ± 1.515	81.5 ± 2.051	0.11 ± 0.012

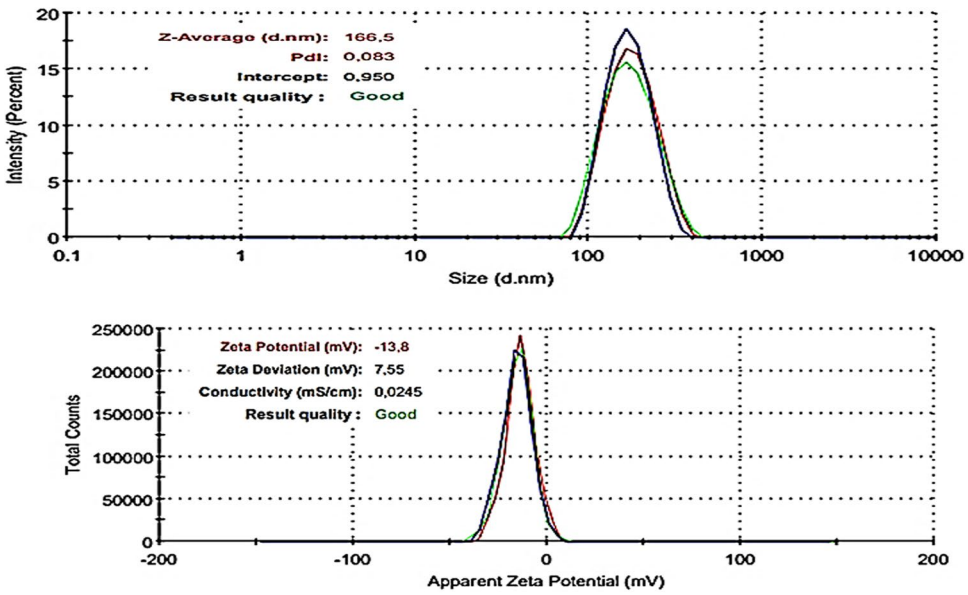

Fig. 2 PBC-PLGA 301 size and zeta potential distribution curves

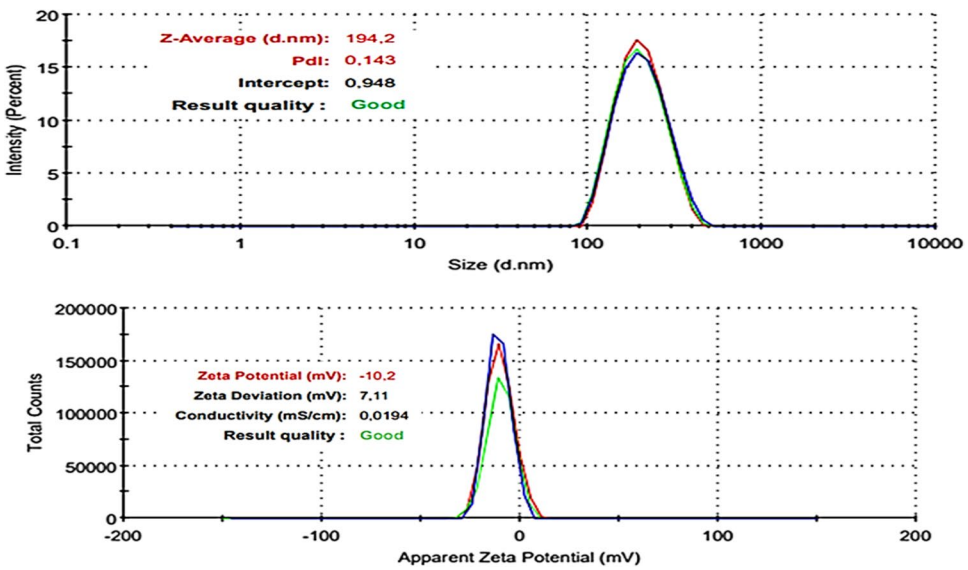

Fig. 3 PBC-PLGA 302 size and zeta potential distribution curves

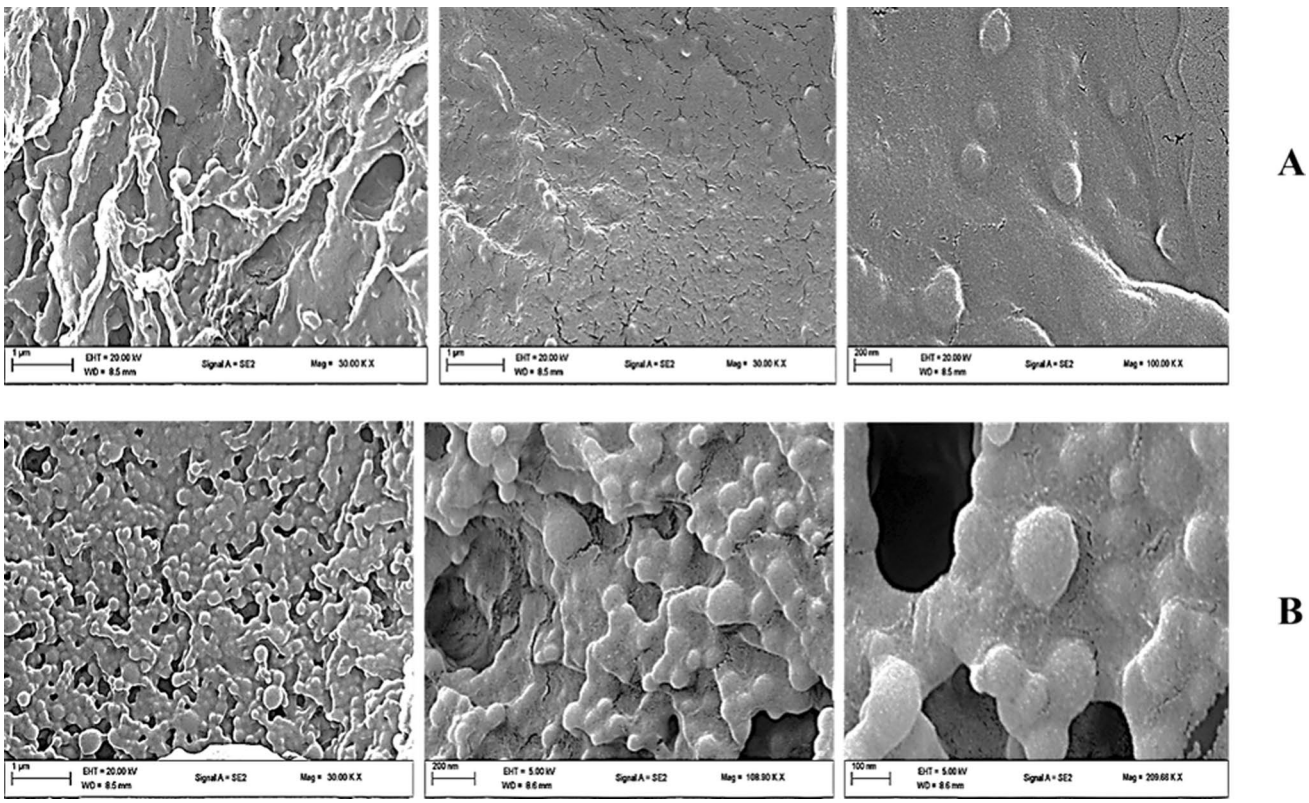

Fig. 4 SEM diagrams of the optimized nanoparticles: PBC-PLGA 301 (**A**) and PBC-PLGA 302 (**B**)

on the nanoformulations of some pyrazolone-based derivatives (68.16 ± 0.67 and 112.1 ± 10.7) [45, 46], they are very much in agreement with the observed sizes (100–250 nm) for most PLGA nanoparticles [13, 47].

The PDI, which ranges from 0 to 2, determines particle homogeneity. When a sample's value approaches 0, it becomes exceedingly homogeneous [48]. As a pointer to uniform particle distribution, samples with homogeneous and equally sized particles would have a lower PDI value, whereas samples with a more diverse range of particle sizes would have a higher PDI value [49]. A minimum PDI is required to maintain the drug release rate consistent and

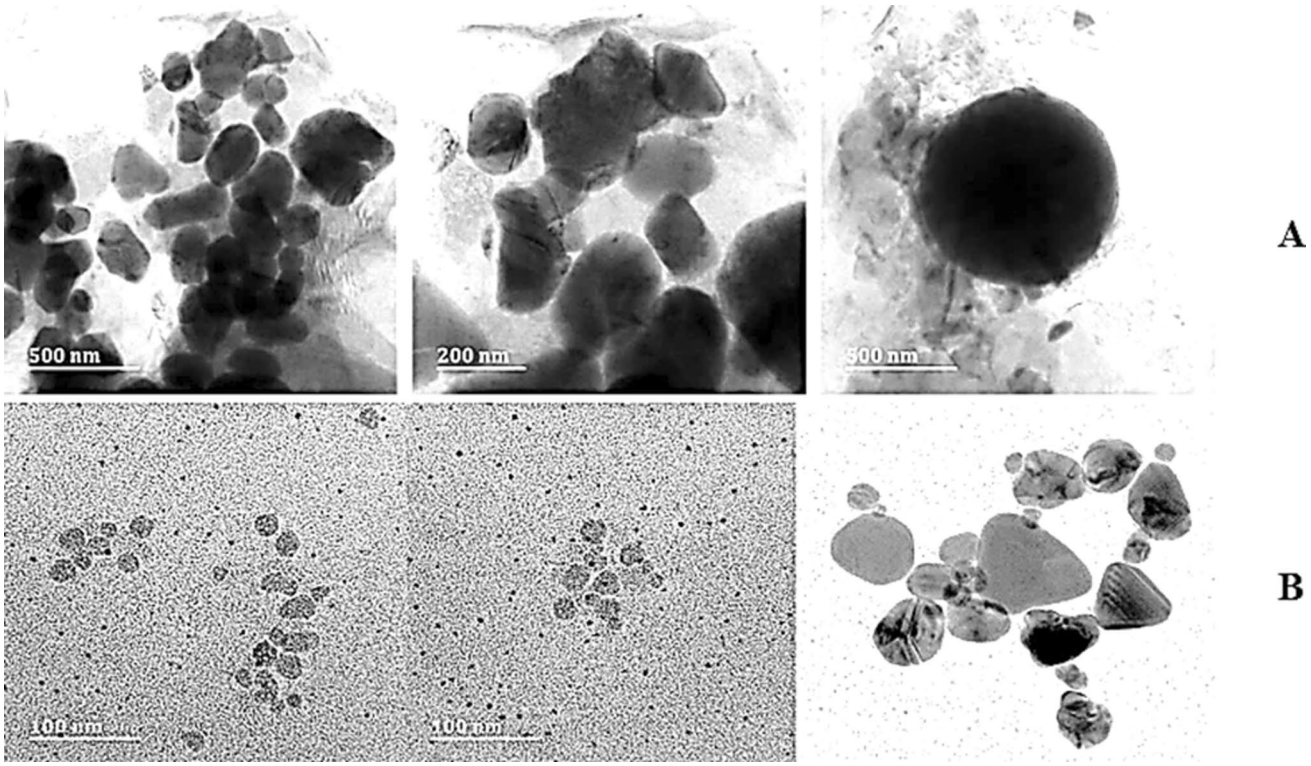

Fig. 5 TEM diagrams of the optimized nanoparticles: PBC-PLGA 301 (**A**) and PBC-PLGA 302 (**B**)

regulated. As shown in Table 1, the PDI of all the nanoparticles varied from 0.12 to 0.14, indicating a homogeneous particle size distribution.

On the other hand, the zeta potential (ζ) indicates the stability of water-based formulations and is based on the mobility of charged particles as measured by an electrical potential. A ZP of $> +30$ mV and -30 mV is desirable for the physical stability of any nanosuspension, with particle charge generally acting as the deciding factor [50]. It also quantifies the strength of the charge repulsion/attraction between particles, a crucial component in processes including flocculation, aggregation, and dispersion [51], and based on the polymer type and the surface functionalization, the zeta potential values may well be positive, neutral, or negative [52]. Neutral nanoparticles have a zeta potential between -10 and $+10$ mV, while strongly cationic and strongly anionic nanoparticles have a zeta potential of higher than $+30$ mV and less than -30 mV, respectively [53]. Surface charges greatly influence nanoparticle uptake and interactions with cells. Nanoparticles with positive charges are more internalizable owing to ionic interactions with negatively charged cell membranes [54, 55]. As a result, they demonstrate perinuclear localization and can escape from lysosomes after being internalized. The lysosome, in contrast, is where negatively and neutrally charged nanoparticles like to co-localize [56]. The PBC-PLGA nanoparticles in this investigation had negatively charged zeta potentials of -14.14 ± 2.900 mV and -10.77 ± 1.515 mV, respectively. These zeta potentials are similar to the finding (-16.87 ± 1.10 mV) observed with AMPDC, a pyrazolone derivative, encapsulated using PLGA/PEG [46]. Interestingly, Alfei and his colleagues noticed a positive zeta potential ($+28.9$ mV) when a bioactive pyrazole derivative was enclosed in a dendrimer. The negative charge on the nanoparticles could be attributed to the PLGA used in the formulation. However, the adsorbed poloxamer could also play a role, as it has previously been reported that it can alter the physicochemical parameters of nanoparticles [57, 58] and may be responsible for the decreased zeta potential. As a result of these ZP values, the nanoparticle was verified to be highly anionic and capable of co-localization with lysosomes. The results also validated the formulations' physical stability.

SEM and TEM images were captured and displayed in Figs. 4 and 5 to corroborate the development of distinct and nanosized particles. PBC-PLGA 301 and PBC-PLGA 302 SEM and TEM pictures indicated that the produced nanoparticles are discrete and spherical with a smooth surface.

3.3 Entrapment Efficiency and Drug-Loading Capacity

The described HPLC method was used to measure entrapment efficiency and drug-loading capacity, and results were derived using Eqs. 1 and 2, with Table 1 summarizing the findings. All particle systems have two important parameters: entrapment efficiency and drug-loading capacity. The proportion of PBC encapsulated in the particles to the total amount of the chemical employed in the preparation is denoted by EE. As a result, it indicates the method's yield for active material. Drug leakage from nanoparticles owing to an incorrectly designed production procedure, formulation variables, or drug degradation during the preparation process may all contribute to EE reduction [59, 60].

On the other hand, the loading capacity (LC) is the proportion of the drug loaded in the nanoparticles to the overall mass. LC is connected to the drug's dose, solubility profile, and degradation of the nanoparticles. For most nanomedicines, high encapsulation efficiency is easier to achieve than high drug-loading capacity [37]. In nanoprecipitation, the polymer mostly encapsulates the medication through noncovalent hydrophobic interactions. According to reports, the majority of PLGA nanoparticle systems have a relatively low drug loading (< 10%), and coming up with ways to improve it is still difficult [61]. The LC of PLGA derivatives is affected by molar mass, chain structure, and the type of the polymer's end groups.

Compounds I and II were successfully incorporated into nanoparticles with excellent cumulative efficiency of 84.20 ± 0.930% and 81.5 ± 2.051%, respectively, comparable to or perhaps greater than some previous studies in the literature on PLGA nanoparticle carriers. For example, average encapsulation efficiency of 60–70% for drugs like estradiol and xanthones and 60–90% for dexamethasone and paclitaxel has been reported [9]. Despite having high encapsulation efficiency, the nanoparticle system showed low loading capacities of 0.30% and 0.11% for PBC-301 and PBC-302, respectively. PLGA macromolecular chains may only slightly expand in aqueous conditions to entrap the chemical, which might account for poor drug loading. Nucleic acid–encapsulated PLGA nanoparticles have been reported to have low loading capacity in the range of 0.1 to 1 mg per 100 mg nanoparticles [62].

3.4 In Vitro Drug Release Study

The release of pyrazolone-based compounds from PBC-PLGA nanoformulations was studied in 7.4 PBS at 37 °C for 48 h, with the cumulative fraction released/dissolved shown in Fig. 6. Drug release from PLGA nanoparticles is a complicated process influenced by several parameters, including polymer degradation, molecular weight, polymer-drug

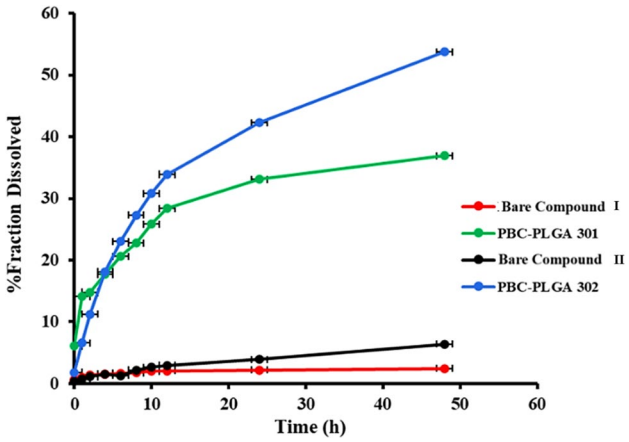

Fig. 6 Comparison of the cumulative percentage fraction dissolved from PBC-PLGA 301 and PBC-PLGA 302 nanoformulations with the bare CompoundsI and II (mean ± SD, $n = 3$)

binding affinity, diffusion rate, protective layer stability, and the drug's physicochemical characteristics.

When compared to the bare compounds, the PBC-PLGA NPs showed a biphasic release pattern: an initial quick release over the first 10 h, followed by a steady, continuous release over a lengthy period (48 h). In 48 h, 2.5 and 6.4% of non-encapsulated compounds were dissolved. However, between 37 and 53% of the chemicals were released from the nanoparticles at the same time. This delay in release time might be attributable to the slow degradation of PLGA, implying that the compound release from nanoparticles is dependent on the pace at which the compounds diffuse from the PLGA surface/matrix, as well as bulk erosion or swelling of the polymer [63]. The strong hydrophobic interactions of the compounds with PLGA, which further prevented a quick release of the compounds from NPs, may have contributed to the extended-release pattern in this investigation.

Additionally, the dissolution pattern of the nanoparticles revealed a burst release during the first 10 h of the investigation, followed by a lag phase of relatively gradual release, which is well documented in the literature regarding PLGA nanoparticles [38, 46, 64]. This first burst impact is due to the instant release/dissolution of the medications that have been adsorbed to the surface and those that are close to the surface of the nanoparticles, which can help swiftly slow the course of a disease state.

The release curves indicated that PBC-PLGA 301 released more slowly than PBC-PLGA 302; this may be attributed to the lower aqueous solubility of Compound I compared to II. In the first 3 h of the investigation, the cumulative release percentage of PBC-PLGA 301 was greater than that of PBC-PLGA 302, which can be ascribed to the adsorption of more compounds to the surface of the nanoparticles. However, at 48 h, the cumulative release of

PBC-PLGA 301 from the nanoparticles was lower than that of PBC-PLGA 302, indicating that Compound II solubility was better improved.

3.4.1 Drug Release Kinetics

Drug dissolution modeling helps identify the mathematical model that best describes the drug release kinetics from drug formulations [65]. In this study, the drug release data for the PBC-PLGA nanoformulations were therefore fitted using five different models: zero-order release, first-order release, Higuchi, Weibull, and Korsmeyer-Peppas models. Table 2 shows the *R*-squared (R^2) values obtained from fitting the dissolution data into each of these models. The closer the *R*-squared value is to 1, signifies the suitability of the model in describing the release mechanism of the formulations.

For PBC-PLGA 301, the Weibull model provided the best fit, with a high R^2 value of 0.972, indicating that the drug release followed a strongly time-dependent mechanism [66]. The Korsmeyer-Peppas model also showed a good fit ($R^2 = 0.920$) with a diffusional exponent (n) of 0.275 for this formulation, suggesting that the release mechanism was primarily governed by Fickian diffusion. The zero-order and first-order models had negative R^2 values, indicating that they are not appropriate for describing the release kinetics of this formulation.

Conversely, for PBC-PLGA 302, the Weibull model showed excellent fit ($R^2 = 0.994$), suggesting a highly predictable and time-dependent release. The Higuchi model also had a strong fit ($R^2 = 0.976$), indicating that diffusion plays a significant role in the release process. The Korsmeyer-Peppas model gave an R^2 of 0.958 with an n value of 0.436, pointing toward anomalous (non-Fickian) transport, likely a combination of diffusion and erosion mechanisms [67]. The zero-order and first-order models had poorer fits compared to the Higuchi, Weibull, and Korsmeyer-Peppas models, with R^2 values of 0.343 and 0.700, respectively.

The results strongly suggest that drug release from the PBC-PLGA 301 and PBC-PLGA 302 formulations are best fitted into the Weibull model denoting a complex and time-dependent drug release behavior. This release behavior may be attributed to the polymer's erosion and degradation processes [68]. Recent studies also have shown that the Weibull model can effectively describe the drug release profile of PLGA-based formulations, capturing the initial burst release, followed by a slower more controlled release phase [68, 69]. This makes the model a valuable tool for predicting and optimizing the performance of PLGA-based drug delivery systems [70, 71].

3.5 Differential Scanning Calorimeter (DSC)

The samples were subjected to DSC analysis to test for structural interference between the polymer and medication and to look at the development of solid-state complexes. The DSC results showed that Compounds I and II were successfully encapsulated within a carrier polymer (PLGA). Individual peaks of each chemical (the bioactive substance and the polymer) will show up in the DSC thermogram if the encapsulated bioactive ingredient is not sufficiently integrated into the encasing polymer, as shown in the literature [72]. No compound peak was seen in the PBC-PLGA nanoparticles thermogram, as shown in Fig. 7(A, B), indicating that Compounds I and II were in their disordered crystalline phase. The fact that the thermograms of PBC-PLGA nanoparticles lack the typical melting and crystalline peaks indicates that the compounds were efficiently enclosed in the PLGA/poloxamer complex.

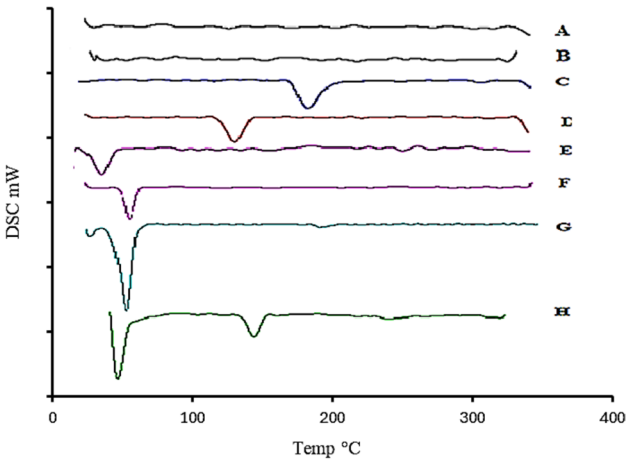

Fig. 7 DSC thermogram of the bare compounds, excipients, and lyophilized nanoparticles. **A** PBC-PLGA 301, **B** PBC-PLGA 302, **C** Compound I, **D** Compound II, **E** PLGA, **F** poloxamer, **G** Compound I physical mixture, and (**H**) Compound II physical mixture

Table 2 Fitting results of drug release kinetics

Sample	Coefficient of determination R^2					Korsmeyer-Peppas
	Zero-order	First-order	Higuchi	Weibull	R^2	Diffusional exponent (n)
PBC-PLGA 301	−1.186	−0.611	0.577	0.972	0.920	0.275
PBC-PLGA 302	0.343	0.700	0.976	0.994	0.958	0.436

3.6 Stability Study

The stability studies of PBC-PLGA NPs 301 and 302 were conducted by assessing the particle size, PDI, and zeta potential over a period of 90 days at two storage conditions: 4 °C and 25 °C. Table 3 summarizes the stability results at refrigerated and at room temperature over a period of 3 months.

As observed from the results, PBC-PLGA 301 particle size remained stable across both storage conditions, fluctuating only slightly between 166 and 171 nm. The PDI decreased from 0.13 to 0.10 at 4 °C, indicating improved homogeneity over time, and remained relatively consistent at 25 °C. However, more significant changes were observed in the zeta potential (ZP), particularly at 25 °C, where it decreased to − 23 mV by day 30. On the other hand, the particle size for PBC-PLGA 302 showed minimal variation, remaining between 186 and 194 nm under both conditions. At 4 °C, the PDI temporarily increased to 0.21 by day 30 but stabilized to 0.06 by day 90. At 25 °C, the PDI was more stable, with a notable decrease to 0.04 by day 60, also signifying increased homogeneity. The ZP exhibited greater variation at 25 °C, dropping to − 23 mV by day 30. Overall, both formulations demonstrated stable particle size at both temperatures, with PBC-PLGA 302 showing better PDI stability at 25 °C. The result implies that the developed formulations are physically stable over time and can be stored at both refrigerated and room temperatures. However, the observed fluctuations in ZP, especially at room temperature, suggest potential issues with long-term colloidal stability for both formulations [73]. Therefore, we recommend prolonging the stability study as well as including other stability-indicating parameters such as chemical stability in the assessment.

3.7 Antimicrobial Activity

Testing for antibacterial activity against *Pseudomonas aeruginosa* (PA), *Escherichia coli* (EC), *Staphylococcus aureus* (SA), *and Methicillin-resistant Staphylococcus aureus* (MRSA) was done on the bare pyrazolone-based compounds and their nanoformulations. Vancomycin was utilized in the test for MRSA, whereas ciprofloxacin was used as the conventional medication for PA, EC, and SA. Higher MIC values denote poor antibacterial activity, and Table 4 summarizes the minimum inhibitory concentration (MIC) values used to assess the antimicrobial activities of the test substances.

From the result, MIC values showed that PBC-PLGA nanoformulations outperformed the bare compounds with respect to antibacterial activity against *E. coli*, *S. aureus*, and MRSA. The MIC obtained for MRSA was comparable to the standard vancomycin, thus proposing the nanoformulations (PBC-PLGA 301 and PBC-PLGA 302) to be better targeted against MRSA. However, all the test samples

Table 3 The results of PBC-PLGA NPs stability over 90 days at 4 °C and 25 °C (mean ± SD, $n = 3$)

Storage condition	Time (day)	PBC-PLGA 301			PBC-PLGA 302		
		Evaluation parameters			Evaluation parameters		
		Size	PDI	ZP	Size	PDI	ZP
4 °C	0	167	0.13	− 14	193	0.13	− 11
	7	171	0.11	− 14	194	0.11	− 15
	30	169	0.12	− 22	194	0.21	− 15
	60	166	0.11	− 17	194	0.04	− 16
	90	168	0.10	− 17	191	0.06	− 13
25 °C	0	167	0.13	− 14	193	0.13	− 11
	7	169	0.13	− 12	191	0.16	− 18
	30	166	0.10	− 23	188	0.14	− 23
	60	166	0.10	− 21	192	0.04	− 14
	90	171	0.12	− 19	186	0.07	− 12

Table 4 Minimum inhibitory concentration (MIC) of the non-encapsulated PBC and their nanoformulations (µg/mL)

Organisms	Test samples					
	I	II	PBC-PLGA 301	PBC-PLGA 302	CIPRO	VCM
P. aeruginosa	62.5	62.5	92	61	0.49	–
E. coli	125	125	15.25	30.5	0.49	–
S. aureus	62.5	62.5	11.25	**7.63**	0.49	–
MRSA	125	31.25	**0.95**	**1.406**	–	3.9

showed minimal activity against *P. aeruginosa* at 62.5 µg/mL for the bare compounds, 92 µg/mL for PBC-PLGA 301, and 61 µg/mL for PBC-PLGA 302, respectively. Studies have demonstrated that the core moiety of the drug, the substituted functional groups, and the kind of cell membranes possessed by the bacteria all affect the antibacterial action. Previous research has shown that compounds similar to pyrazole/hydrazo-thiazole moiety have antibacterial action [74–76]. When comparing the MIC values from the bare compounds to their nanoformulations, it can be deduced that increasing the solubility of the compounds improved their antimicrobial activity against *E. coli*, *S. aureus*, and MRSA. This finding is consistent with a prior study by Alfei and Sun et al. confirming that increasing solubility improved bioactivity [45, 46].

3.8 Bacterial Cell Membrane Permeability

MRSA and SA bacterial cells were treated for 24 h with the nanoformulations (PBC-PLGA 301 and PBC-PLGA 302) and standard drugs (ciprofloxacin and vancomycin). The PI dye assessed the cell death caused by the nanoformulations. The PI dye is a membrane-impermeable dye typically repelled by living cells. It attaches to double-stranded DNA by intercalating between the base pairs, and its detection indicates either membrane permeability or cell death. In this study, ciprofloxacin was used as the control for SA, and VCM was used as the control drug for MRSA to indicate cellular uptake or cell death. VCM compromises the integrity of the cell wall, enhancing PI permeability and uptake. Samples were taken from wells 6 and 5 for SA and MRSA, respectively. The data was then captured and analyzed using Kaluza 2.1 (Beckman Coulter, USA) flow cytometer software. As seen in Fig. 8, the PI fluorescence changed when the nanoformulations and conventional control medications were applied to the bacterial cell. The results showed that the PBC-PLGA nanoformulations exhibited higher levels of cell membrane permeability than popular drugs, vancomycin and ciprofloxacin. The nanoformulations moreover demonstrated improved permeability of higher than 90% into SA compared to the MRSA, which is slightly less than 90% for PBC-PLGA 302 and 86% for PBC-PLGA 301. These findings imply that nanoformulations may be useful antibacterial medicines since they penetrate better than conventional medications.

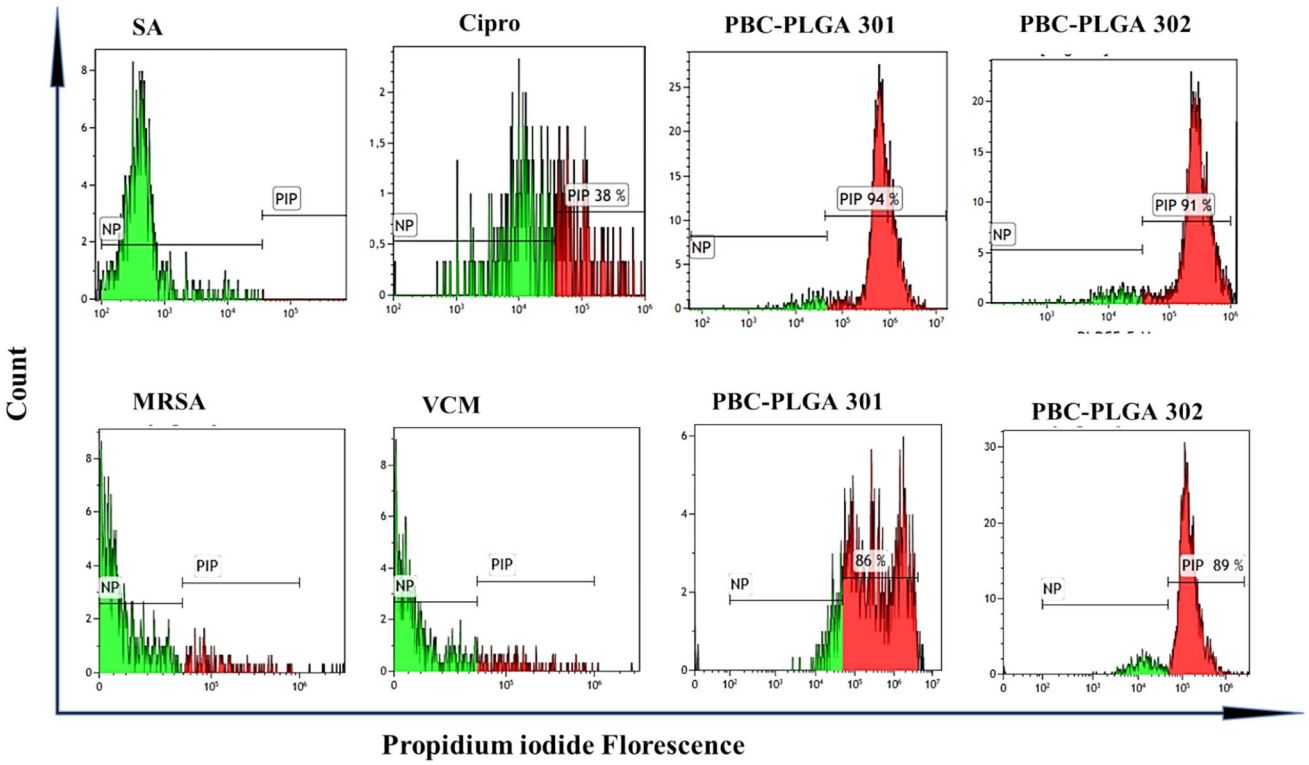

Fig. 8 Cell counts vs. propidium dye uptake. Green represents untreated SA/MRSA (not PI permeable); red represents the percentage of uptake in the population after incubation with Cipro, VCM, PBC-PLGA 301, and PBC-PLGA 302

3.9 In Vitro Hemolysis Study

Pharmaceutical scientists typically employ the hemolysis assay to illustrate a product's toxicity in blood circulation. Therefore, it is argued that hemolysis occurs when RBCs break down, releasing the contained hemoglobin into the surrounding medium. Hence, a nanoformulation must have little interaction with circulatory constituents and remain stable over time. According to the "American Society for Testing and Materials" (ASTMF 756–00, 2000), materials are divided into three categories: hemolytic (hemolysis over 5%), somewhat hemolytic (hemolysis between 2 and 5%), and non-hemolytic (below 2%) [30, 77]. In this investigation, the PBC-PLGA nanoformulations were subjected to in vitro hemolysis research using sheep blood. The average hemolysis is shown in Fig. 9. PBC-PLGA 301 was seen in the figure to be non-hemolytic (below 2%), demonstrating that the formulation is extremely hemocompatible. However, the PBC-PLGA 302 formulation had minimal hemolysis, with an average of 2 to 5%, indicating that it is only marginally compatible with blood components. A comparable study using PLGA:poloxamer mix nanoparticles found less than 1% hemolysis [78]. Consequently, additional variables like particle type and concentration may be responsible for the minimal interaction between PBC-PLGA 302 and the detected organic blood components. However, these particles' biocompatibility could be enhanced by being coated in hydrophilic polymers like PEG [79].

3.9.1 Radical Scavenging Activity

Free radicals are very reactive and unstable species that develop during numerous metabolic processes and harm live cells, breaking DNA and causing strand breaks [80]. These free radicals are strongly linked to oxidative stress, cancer, hepatic and vascular illness, inflammatory disorders, rheumatoid arthritis, and aging. Significant progress has recently been achieved in the study of free radicals and the creation of antioxidants. Antioxidant molecules stop free radicals from stealing electrons from other molecules, preventing the molecule from becoming unstable and suffering oxidative damage [81].

This study used gallic acid as the reference material to assess the DPPH, FRAP, and NO scavenging activity of Compounds I, II, and PBC-PLGA nanoparticles. Data are presented as mean ± SEM.

Results from this study showed that the examined pyrazolone-based compounds and their optimized nanoparticles had varying rates of DPPH, FRAP, and NO scavenging, as shown in Figs. 10 and 11(A, B, and C), respectively, with the tested components showing a dose-dependent radical scavenging activity. Gallic acid outperformed the new pyrazolone-based compounds at various concentrations, with a modest scavenging activity of less than 40% with DPPH. Although activity was less than 20% at all test doses with NO, there were no significant differences between the bare compounds and gallic acid for the FRAP and NO testing. The IC_{50} values obtained in the three assays (Fig. 12A, B) further proved that Compound I, with an average of 4.6, has superior FRAP scavenging activity than the standard antioxidant (gallic acid 6.2) and is a better antioxidant when compared to Compound II, in all three assays. Both compounds have the pyrazolyl-thiazole moiety and the hydrazo linkage, which have previously been linked to antioxidant action [82–85], suggesting that these moieties may be responsible for their radical scavenging action.

On the other hand, in Fig. 11A, B, and C, the antioxidant efficacy of PBC-PLGA nanoparticles was demonstrated in the experiments. In the DPPH assay, the PBC-PLGA 301 and PBC-PLGA 302 nanoparticles at higher 15–60 µg/mL concentrations exhibited solid antioxidant activity (70–80%) compared to the standard gallic acid (50%), which is not so at lower concentrations. However, there are no significant differences in the DPPH scavenging activity of PBC-PLGA

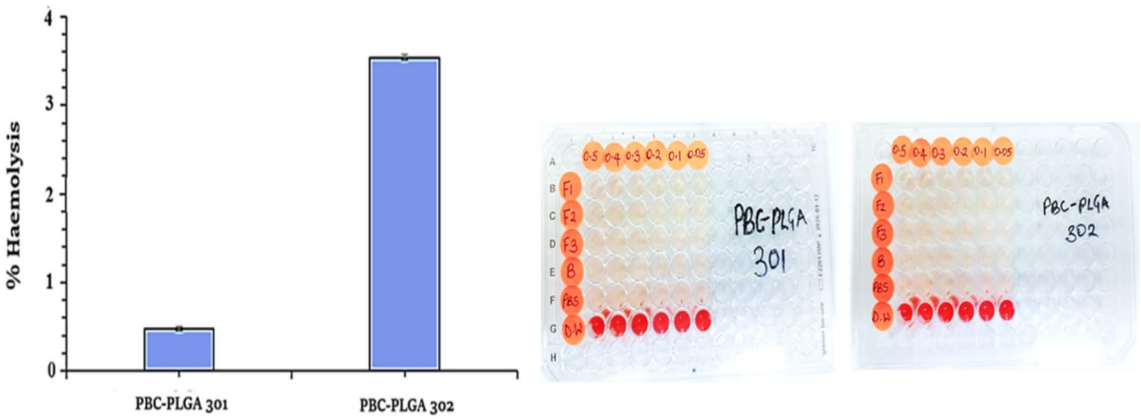

Fig. 9 Percentage hemolysis of PBC-PLGA nanoformulations and pictorial representation of the samples

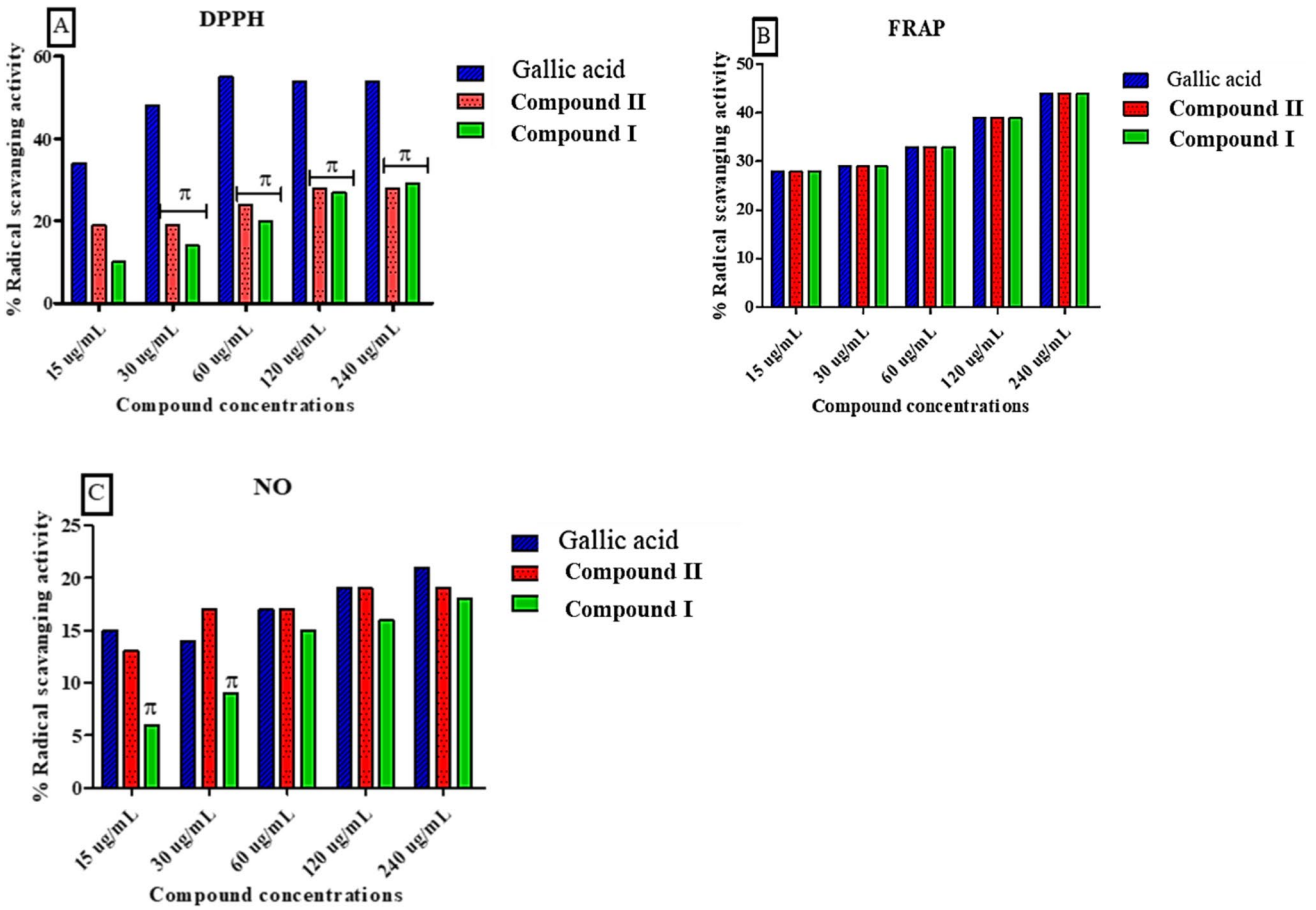

Fig. 10 **A**–**C** Radical scavenging activity of novel Compounds I and II against DPPH, FRAP, and NO

301 and PBC-PLGA 302 at different concentrations. The nanoparticles showed better Ferric-reducing ability at all test concentrations than gallic acid in the FRAP assay. Also, the antioxidant power of the PBC-PLGA 301 and 302 nanoparticles are comparable at all test concentrations as no significant difference was observed, and both attained a maximum scavenging activity of 70% at the highest test concentration. While the test samples indicated strong antioxidant power with DPPH and FRAP assays, they appeared to have moderate NO scavenging activity (maximum of 50%) in a dose-dependent manner. There was no significant difference in the NO scavenging activity of PBC-PLGA nanoparticles and the antioxidant standard gallic acid. The IC_{50} values of the nanoparticles in the different assays (Fig. 12) further substantiated the percentage scavenging activity in Figs. 10 and 11. Generally, the nanoformulations showed improved and better antioxidant activity at lower concentrations than the bare compounds, as an approximately threefold increase in percentage scavenging activity was observed in all assays.

4 Conclusion

Poor solubility is a significant barrier to the clinical translation of many new drug candidates. In this study, water-soluble nanoformulations were efficiently developed for two novel pyrazolone compounds. The developed formulation possessed optimum physicochemical properties with significant biocompatibility, exhibiting enhanced antioxidant and antibacterial activities compared to the bare compounds and standard drugs. A significant bacterial cell death was also observed, indicating they may be used as bactericidal agents. With these promising results, nanoformulations of the pyrazolone-based derivatives can be employed as potential pharmaceutical agents to treat bacterial infections and other oxidative stress-related ailments. However, future studies involving animal models and clinical trials need to be done to establish their clinical applications.

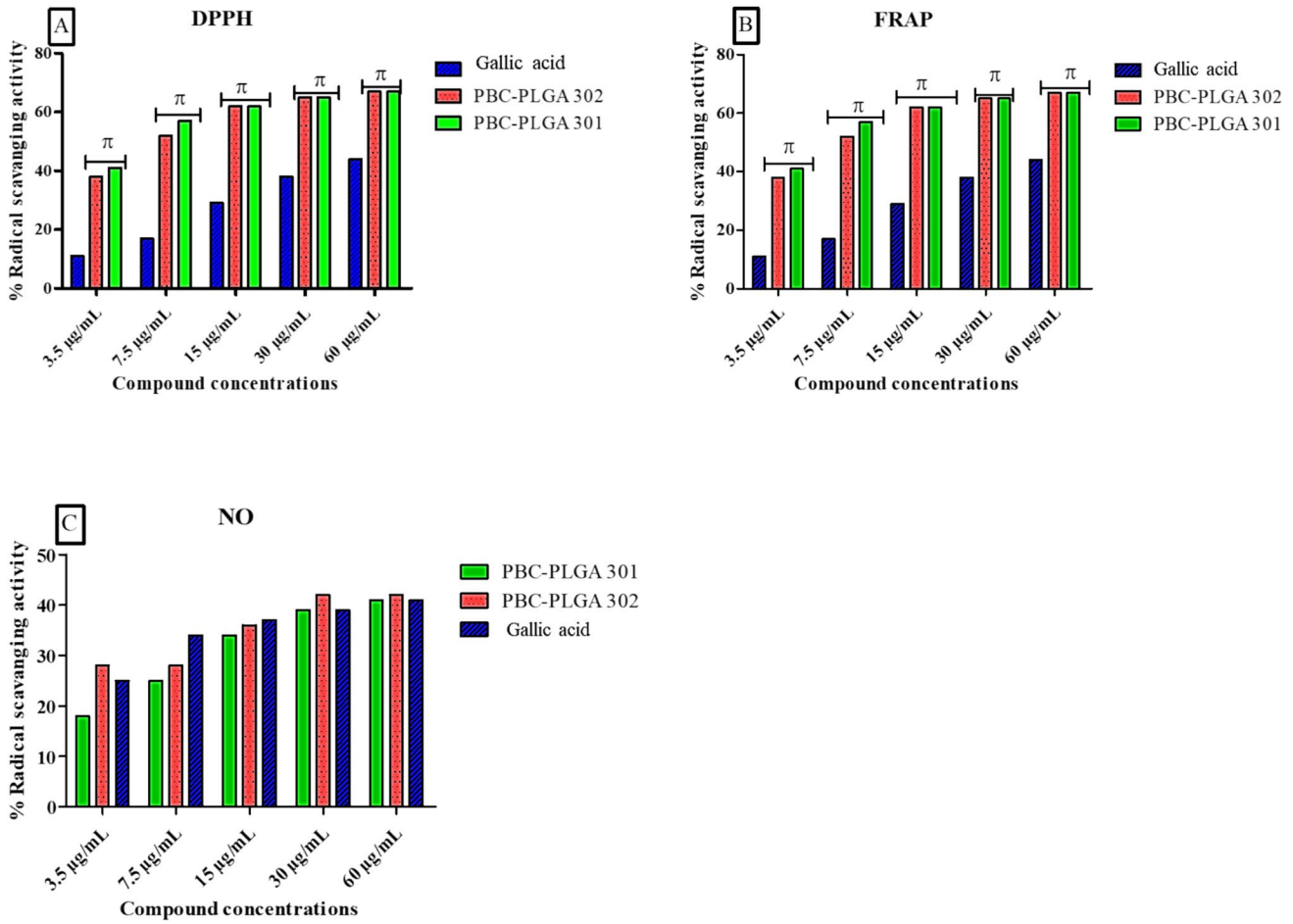

Fig. 11 **A**–**C** Radical scavenging activity of PBC-PLGA 301 and PBC-PLGA 302 nanoformulations against DPPH, FRAP, and NO

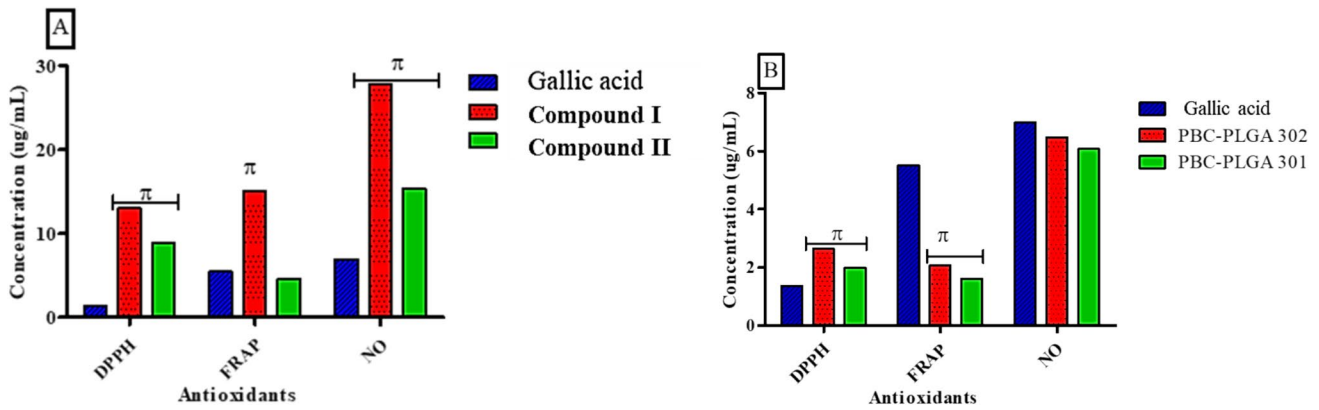

Fig. 12 IC_{50} values of biological activities exhibited by the bare Compounds I and II (**A**) and the PBC-PLGA nanoparticles (**B**) on different antioxidant parameters

Supplementary Information The online version contains supplementary material available at https://doi.org/10.1007/s12668-024-01675-8.

Acknowledgements The authors acknowledge the support of the Pharmaceutical Microbiology Lab (Sithabile Mokoena), Blessing Ike, Mohammed Mshelia, the UKZN Nanotechnology Platform, the Microscopy and Microanalysis Unit, the Department of Human Physiology, and the Flow Cytometry Research Laboratory for their invaluable assistance in the course of this research.

Author Contribution N.N.I.: conceptualization, data curation, investigation, formal analysis, validation, and writing—original draft preparation; E.A.IA.: conceptualization, writing—review and editing; V.A.O.: design, synthesis, and characterization of Compounds I and II; A.N.: flow cytometry analysis; M.G.: edited the manuscript and figures; R.K.: supervision; M.F.: supervision

Funding Open access funding provided by University of KwaZulu-Natal.

Data Availability No datasets were generated or analysed during the current study.

Declarations

Competing Interest The authors declare no competing interests.

Research Involving Humans and Animals Statement None.

Informed consent All authors consent to the publication of this article. The research does not involve humans or animals.

References

1. Xie, Y., & Yao, Y. (2018). Octenylsuccinate hydroxypropyl phytoglycogen, a dendrimer-like biopolymer, solubilizes poorly water-soluble active pharmaceutical ingredients. *Carbohydrate polymers, 180*, 29–37.
2. Abdelkader, H., & Fathalla, Z. (2018). Investigation into the emerging role of the basic amino acid L-lysine in enhancing solubility and permeability of BCS class II and BCS class IV drugs. *Pharmaceutical Research, 35*, 1–18.
3. Sugano, K., Okazaki, A., Sugimoto, S., Tavornvipas, S., Omura, A., & Mano, T. (2007). Solubility and dissolution profile assessment in drug discovery. *Drug Metabolism and Pharmacokinetics, 22*, 225–254.
4. Sharma, M., Sharma, R., & Jain, D. K. (2016). Nanotechnology based approaches for enhancing oral bioavailability of poorly water soluble antihypertensive drugs. *Scientifica, 2016*(1), 8525679.
5. Kumar, S., Dilbaghi, N., Saharan, R., & Bhanjana, G. (2012). Nanotechnology as emerging tool for enhancing solubility of poorly water-soluble drugs. *BioNanoScience, 2*, 227–250.
6. Khan, K. U., Minhas, M. U., Badshah, S. F., Suhail, M., Ahmad, A., & Ijaz, S. (2022). Overview of nanoparticulate strategies for solubility enhancement of poorly soluble drugs. *Life Sciences, 291*, 120301.
7. Babadi, D., Dadashzadeh, S., Osouli, M., Abbasian, Z., Daryabari, M. S., Sadrai, S., & Haeri, A. (2021). Biopharmaceutical and pharmacokinetic aspects of nanocarrier-mediated oral delivery of poorly soluble drugs. *Journal of Drug Delivery Science and Technology, 62*, 102324.
8. Zhang, S., Wu, Y., He, B., Luo, K., & Gu, Z. (2014). Biodegradable polymeric nanoparticles based on amphiphilic principle: Construction and application in drug delivery. *Science China Chemistry, 57*, 461–475.
9. Kumari, A., Yadav, S. K., & Yadav, S. C. (2010). Biodegradable polymeric nanoparticles based drug delivery systems. *Colloids and Surfaces B: Biointerfaces, 75*, 1–18.
10. Hwang, D., Ramsey, J. D., & Kabanov, A. V. (2020). Polymeric micelles for the delivery of poorly soluble drugs: From nanoformulation to clinical approval. *Advanced Drug Delivery reviews, 156*, 80–118.
11. Lu, Y., Cheng, D., Niu, B., Wang, X., Wu, X., & Wang, A. (2023). Properties of poly (lactic-co-glycolic acid) and progress of poly (lactic-co-glycolic acid)-based biodegradable materials in biomedical research. *Pharmaceuticals, 16*, 454.
12. Fatma, S., Talegaonkar, S., Iqbal, Z., Panda, A. K., Negi, L. M., Goswami, D. G., & Tariq, M. (2016). Novel flavonoid-based biodegradable nanoparticles for effective oral delivery of etoposide by P-glycoprotein modulation: An in vitro, ex vivo and in vivo investigations. *Drug Delivery, 23*, 500–511.
13. Danhier, F., Ansorena, E., Silva, J. M., Coco, R., Le Breton, A., & Préat, V. (2012). PLGA-based nanoparticles: An overview of biomedical applications. *Journal of Controlled Release, 161*, 505–522.
14. Jain, R. A. (2000). The manufacturing techniques of various drug loaded biodegradable poly (lactide-co-glycolide)(PLGA) devices. *Biomaterials, 21*, 2475–2490.
15. Bobo, D., Robinson, K. J., Islam, J., Thurecht, K. J., & Corrie, S. R. (2016). Nanoparticle-based medicines: A review of FDA-approved materials and clinical trials to date. *Pharmaceutical Research, 33*, 2373–2387.
16. Wang, Y., Qin, B., Xia, G., & Choi, S. H. (2021). FDA's poly (lactic-co-glycolic acid) research program and regulatory outcomes. *The AAPS Journal, 23*, 92.
17. Anwer, M. K., Al-Mansoor, M. A., Jamil, S., Al-Shdefat, R., Ansari, M. N., & Shakeel, F. (2016). Development and evaluation of PLGA polymer based nanoparticles of quercetin. *International Journal of Biological macromolecules, 92*, 213–219.
18. Wan, S., Zhang, L., Quan, Y., & Wei, K. (2018). Resveratrol-loaded PLGA nanoparticles: Enhanced stability, solubility and bioactivity of resveratrol for non-alcoholic fatty liver disease therapy. *Royal Society open Science, 5*, 181457.
19. da Silva Feltrin, F., Agner, T., Sayer, C., & Lona, L. M. F. (2022). Curcumin encapsulation in functional PLGA nanoparticles: A promising strategy for cancer therapies. *Advances in Colloid and Interface Science*, 300, 102582.
20. Elsewedy, H. S., Dhubiab, B. E. A., Mahdy, M. A., & Elnahas, H. M. (2020). Development, optimization, and evaluation of PEGylated brucine-loaded PLGA nanoparticles. *Drug Delivery, 27*, 1134–1146.
21. Verma, R., Verma, S. K., Rakesh, K. P., Girish, Y. R., Ashrafizadeh, M., Kumar, K. S. S., & Rangappa, K. S. (2021).

Pyrazole-based analogs as potential antibacterial agents against methicillin-resistance staphylococcus aureus (MRSA) and its SAR elucidation. *European Journal of Medicinal Chemistry, 212*, 113134.
22. Karrouchi, K., Radi, S., Ramli, Y., Taoufik, J., Mabkhot, Y.N., Al-Aizari, F.A., Ansar, M.h. (2018). Synthesis and pharmacological activities of pyrazole derivatives: A review. *Molecules, 23(1),* 134.https://doi.org/10.3390/molecules23010134
23. Jamwal, A., Javed, A., & Bhardwaj, V. (2013). A review on pyrazole derivatives of pharmacological potential. *J. Pharm. BioSci, 3*, 114–123.
24. Wu, T.-W., Zeng, L.-H., Wu, J., & Fung, K.-P. (2002). Myocardial protection of MCI-186 in rabbit ischemia–reperfusion. *Life sciences, 71*, 2249–2255.
25. Masih, A., Agnihotri, A. K., Srivastava, J. K., Pandey, N., Bhat, H. R., & Singh, U. P. (2021). Discovery of novel pyrazole derivatives as a potent anti-inflammatory agent in RAW264. 7 cells via inhibition of NF-κB for possible benefit against SARS-CoV-2. *Journal of biochemical and molecular toxicology, 35*, e22656.
26. Chen, L., Chen, S., Gui, C., Shen, J., Shen, X., & Jiang, H. (2006). Discovering severe acute respiratory syndrome coronavirus 3CL protease inhibitors: Virtual screening, surface plasmon resonance, and fluorescence resonance energy transfer assays. *Slas Discovery, 11*, 915–921.
27. Obakachi, V. A., Kushwaha, N. D., Kushwaha, B., Mahlalela, M. C., Shinde, S. R., Kehinde, I., & Karpoormath, R. (2021). Design and synthesis of pyrazolone-based compounds as potent blockers of SARS-CoV-2 viral entry into the host cells. *Journal of Molecular Structure, 1241*, 130665.
28. Obakachi, V. A., Kehinde, I., Kushwaha, N. D., Akinpelu, O. I., Kushwaha, B., Merugu, S. R., Kayamba, F., Kumalo, H. M., & Karpoormath, R. (2022). Structural based investigation of novel pyrazole-thiazole hybrids as dual CDK-1 and CDK-2 inhibitors for cancer chemotherapy. *Molecular Simulation, 48*, 687–701.
29. Yallapu, M. M., Gupta, B. K., Jaggi, M., & Chauhan, S. C. (2010). Fabrication of curcumin encapsulated PLGA nanoparticles for improved therapeutic effects in metastatic cancer cells. *Journal of Colloid and Interface Science, 351*, 19–29.
30. Algharib, S. A., Dawood, A., Zhou, K., Chen, D., Li, C., Meng, K., Maa, M. K., Ahmed, S., Huang, L., & Xie, S. (2020). Designing, structural determination and biological effects of rifaximin loaded chitosan-carboxymethyl chitosan nanogel. *Carbohydrate polymers, 248*, 116782.
31. Ali, H. S., York, P., Ali, A. M., & Blagden, N. (2011). Hydrocortisone nanosuspensions for ophthalmic delivery: A comparative study between microfluidic nanoprecipitation and wet milling. *Journal of controlled release, 149*, 175–181.
32. Allen, J. L., Kennedy, S. J., & Shaw, L. N. (2022). Colorimetric assays for the rapid and high-throughput screening of antimicrobial peptide activity against diverse bacterial pathogens. *Methods in Enzymology*, Elsevier, pp. 131–156.
33. Faya, M., Hazzah, H. A., Omolo, C. A., Agrawal, N., Maji, R., Walvekar, P., Mocktar, C., Nkambule, B., Rambharose, S., & Albericio, F. (2020). Novel formulation of antimicrobial peptides enhances antimicrobial activity against methicillin-resistant Staphylococcus aureus (MRSA). *Amino Acids, 52*, 1439–1457.
34. Oyaizu, M. (1986). Studies on products of browning reaction antioxidative activities of products of browning reaction prepared from glucosamine. *The Japanese journal of nutrition and dietetics, 44*, 307–315.
35. Singh, D., Mishra, M., Gupta, M., Singh, P., Gupta, A., & Nema, R. (2012). Nitric oxide radical scavenging assay of bioactive compounds present in methanol extract of Centella asiatica. *International Journal of Pharmacy and Pharmaceutical Science Research, 2*, 42–44.
36. Wais, U., Jackson, A. W., He, T., & Zhang, H. (2016). Nanoformulation and encapsulation approaches for poorly water-soluble drug nanoparticles. *Nanoscale, 8*, 1746–1769.
37. Snejdrova, E., Loskot, J., Martiska, J., Soukup, T., Prokes, L., Frolov, V., & Kucera, T. (2022). Rifampicin-loaded PLGA nanoparticles for local treatment of musculoskeletal infections: Formulation and characterization. *Journal of Drug Delivery Science and Technology, 73*, 103435.
38. Godara, S., Lather, V., Kirthanashri, S., Awasthi, R., & Pandita, D. (2020). Lipid-PLGA hybrid nanoparticles of paclitaxel: Preparation, characterization, in vitro and in vivo evaluation. *Materials Science and Engineering: C, 109*, 110576.
39. Zhang, E., Osipova, N., Sokolov, M., Maksimenko, O., Semyonkin, A., Wang, M., Grigartzik, L., Gelperina, S., Sabel, B. A., & Henrich-Noack, P. (2021). Exploring the systemic delivery of a poorly water-soluble model drug to the retina using PLGA nanoparticles. *European Journal of Pharmaceutical Sciences, 164*, 105905.
40. Morachis, J. M., Mahmoud, E. A., & Almutairi, A. (2012). Physical and chemical strategies for therapeutic delivery by using polymeric nanoparticles. *Pharmacological reviews, 64*, 505–519.
41. Crucho, C. I., & Barros, M. T. (2017). Polymeric nanoparticles: A study on the preparation variables and characterization methods. *Materials Science and Engineering: C, 80*, 771–784.
42. Snejdrova, E., Dittrich, M., & Drastik, M. (2013). Plasticized branched aliphatic oligoesters as potential mucoadhesive drug carriers. *International journal of pharmaceutics, 458*, 282–286.
43. Ehrenstein, G. W. (2012). *Polymeric materials: Structure, properties, applications*. Carl Hanser Verlag GmbH Co KG.
44. Wang, C., Wang, S., Zhang, B., Zhang, X., Tong, X., Peng, H., Han, X., & Liu, C. (2018). Layering poly (lactic-co-glycolic acid)-based electrospun membranes and co-culture cell sheets for engineering temporomandibular joint disc. *Journal of Biological Regulators and Homeostatic Agents, 32*, 55–61.
45. Alfei, S., Brullo, C., Caviglia, D., & Zuccari, G. (2021). Preparation and physicochemical characterization of water-soluble pyrazole-based nanoparticles by dendrimer encapsulation of an insoluble bioactive pyrazole derivative. *Nanomaterials, 11*, 2662.
46. Sun, X., Zhang, L., Gao, M., Que, X., Zhou, C., Zhu, D., & Cai, Y. (2019). Nanoformulation of a novel pyrano [2, 3-c] pyrazole heterocyclic compound AMDPC exhibits anti-cancer activity via blocking the cell cycle through a P53-independent pathway. *Molecules, 24*, 624.
47. Mora-Huertas, C. E., Fessi, H., & Elaissari, A. (2010). Polymer-based nanocapsules for drug delivery. *International journal of pharmaceutics, 385*, 113–142.
48. Henry, L. J. K., Natesan, S., & Kandasamy, R. (2017). Atrial natriuretic peptide-conjugated chitosan-hydrazone-mPEG copolymer nanoparticles as pH-responsive carriers for intracellular delivery of prednisone. *Carbohydrate polymers, 157*, 1677–1686.
49. Hassan, U. A., Hussein, M. Z., Alitheen, N. B., Ariff, S. A. Y., & Masarudin, M. J. (2018). In vitro cellular localization and efficient accumulation of fluorescently tagged biomaterials from monodispersed chitosan nanoparticles for elucidation of controlled release pathways for drug delivery systems. *International journal of nanomedicine, 13*, 5075.
50. Nallamuthu, I., Devi, A., & Khanum, F. (2015). Chlorogenic acid loaded chitosan nanoparticles with sustained release property, retained antioxidant activity and enhanced bioavailability. *Asian Journal of Pharmaceutical Sciences, 10*, 203–211.
51. Dickinson, E. (2009). Hydrocolloids as emulsifiers and emulsion stabilizers. *Food Hydrocolloids, 23*, 1473–1482.
52. Soppimath, K. S., Aminabhavi, T. M., Kulkarni, A. R., & Rudzinski, W. E. (2001). Biodegradable polymeric nanoparticles as drug delivery devices. *Journal of controlled release, 70*, 1–20.

53. Clogston, J. D., Crist, R. M., & McNeil, S. E. (2016). Physicochemical characterization of polymer nanoparticles: Challenges and present limitations. In Polymer Nanoparticles for Nanomedicines: *A Guide for Their Design, Preparation, and Development* (pp. 187–203).
54. Foged, C., Brodin, B., Frokjaer, S., & Sundblad, A. (2005). Particle size and surface charge affect particle uptake by human dendritic cells in an in vitro model. *International journal of pharmaceutics, 298*, 315–322.
55. Vasir, J. K., & Labhasetwar, V. (2008). Quantification of the force of nanoparticle-cell membrane interactions and its influence on intracellular trafficking of nanoparticles. *Biomaterials, 29*, 4244–4252.
56. Yue, Z.-G., Wei, W., Lv, P.-P., Yue, H., Wang, L.-Y., Su, Z.-G., & Ma, G.-H. (2011). Surface charge affects cellular uptake and intracellular trafficking of chitosan-based nanoparticles. *Biomacromolecules, 12*, 2440–2446.
57. Jain, D., Athawale, R., Bajaj, A., Shrikhande, S., Goel, P. N., & Gude, R. P. (2013). Studies on stabilization mechanism and stealth effect of poloxamer 188 onto PLGA nanoparticles. *Colloids and Surfaces B: Biointerfaces, 109*, 59–67.
58. Santander-Ortega, M. J., Csaba, N., Alonso, M. J., Ortega-Vinuesa, J. L., & Bastos-Gonzalez, D. (2007). Stability and physicochemical characteristics of PLGA, PLGA: Poloxamer and PLGA: Poloxamine blend nanoparticles: A comparative study. *Colloids and Surfaces A: Physicochemical and Engineering Aspects, 296*, 132–140.
59. Alshamsan, A. (2014). Nanoprecipitation is more efficient than emulsion solvent evaporation method to encapsulate cucurbitacin I in PLGA nanoparticles. *Saudi Pharmaceutical Journal, 22*, 219–222.
60. Singh, H., Bhandari, R., & Kaur, I. P. (2013). Encapsulation of rifampicin in a solid lipid nanoparticulate system to limit its degradation and interaction with isoniazid at acidic pH. *International Journal of Pharmaceutics, 446*, 106–111.
61. Liu, Y., Yang, G., Jin, S., Xu, L., & Zhao, C. X. (2020). Development of high-drug-loading nanoparticles. *ChemPlusChem, 85*, 2143–2157.
62. Danhier, F., Feron, O., & Préat, V. (2010). To exploit the tumor microenvironment: Passive and active tumor targeting of nanocarriers for anti-cancer drug delivery. *Journal of controlled release, 148*, 135–146.
63. Mu, L., & Feng, S.-S. (2003). PLGA/TPGS nanoparticles for controlled release of paclitaxel: Effects of the emulsifier and drug loading ratio. *Pharmaceutical Research, 20*, 1864–1872.
64. Pimple, S., Manjappa, A. S., Ukawala, M., & Murthy, R. (2012). PLGA nanoparticles loaded with etoposide and quercetin dihydrate individually: In vitro cell line study to ensure advantage of combination therapy. *Cancer nanotechnology, 3*, 25–36.
65. Askarizadeh, M., Esfandiari, N., Honarvar, B., Sajadian, S. A., & Azdarpour, A. (2023). Kinetic modeling to explain the release of medicine from drug delivery systems. *ChemBioEng Reviews, 10*, 1006–1049.
66. Lakshani, N., Wijerathne, H., Sandaruwan, C., Kottegoda, N., & Karunarathne, V. (2023). Release kinetic models and release mechanisms of controlled-release and slow-release fertilizers. *ACS Agricultural Science & Technology, 3*, 939–956.
67. Aykın-Dinçer, E., Dinçer, C., & Topuz, O. K. (2024). Modeling of release mechanism of sage (Salvia fruticosa Miller) phenolics encapsulated in alginate capsule: Physicochemical properties. *Journal of Food Processing and Preservation, 2024*, 7598455.
68. Lagreca, E., Onesto, V., Di Natale, C., La Manna, S., Netti, P. A., & Vecchione, R. (2020). Recent advances in the formulation of PLGA microparticles for controlled drug delivery. *Progress in Biomaterials, 9*, 153–174.
69. de Jesús Martín-Camacho, U., Rodríguez-Barajas, N., Sánchez-Burgos, J. A., & Pérez-Larios, A.. (2023). Weibull β value for the discernment of drug release mechanism of PLGA particles. *International Journal of Pharmaceutics, 640*, 123017.
70. Rahmani, F., Naderpour, S., Nejad, B. G., Rahimzadegan, M., Ebrahimi, Z. N., Kamali, H., & Nosrati, R. (2023). The recent insight in the release of anticancer drug loaded into PLGA microspheres. *Medical Oncology, 40*, 229.
71. Kırımlıoğlu, G. Y. (2023). Chapter 3 - Drug loading methods and drug release mechanisms of PLGA nanoparticles. In P. Kesharwani (Ed.), *Poly (lactic-co-glycolic acid) (PLGA) Nanoparticles for Drug Delivery* (pp. 55–86). Elsevier.
72. Hadidi, M., Pouramin, S., Adinepour, F., Haghani, S., & Jafari, S. M. (2020). Chitosan nanoparticles loaded with clove essential oil: Characterization, antioxidant and antibacterial activities. *Carbohydrate polymers, 236*, 116075.
73. Shehzad, Q., Liu, Z., Zuo, M., & Wang, J. (2024). The role of polysaccharides in improving the functionality of zein coated nanocarriers: Implications for colloidal stability under environmental stresses. *Food chemistry, 431*, 136967.
74. Sun, Y., Li, Y., & Liu, J. (2023). Mathematical modeling and numerical simulations for drug release from PLGA particles. *International Conference on Computational Science*, Springer, 347–360.
75. Karrouchi, K., Radi, S., Ramli, Y., Taoufik, J., Mabkhot, Y. N., Al-Aizari, F. A., & Ansar, M. H. (2018). Synthesis and pharmacological activities of pyrazole derivatives: A review. *Molecules, 23*, 134.
76. Asif, M., Imran, M., & Husain, A. (2021). Approaches for chemical synthesis and diverse pharmacological significance of pyrazolone derivatives: A review. *Journal of the Chilean Chemical Society, 66*, 5149–5163.
77. Hejjaji, E. M., Smith, A. M., & Morris, G. A. (2018). Evaluation of the mucoadhesive properties of chitosan nanoparticles prepared using different chitosan to tripolyphosphate (CS: TPP) ratios. *International journal of biological macromolecules, 120*, 1610–1617.
78. Gupta, P. N., Jain, S., Nehate, C., Alam, N., Khare, V., Dubey, R. D., Saneja, A., Kour, S., & Singh, S. K. (2014). Development and evaluation of paclitaxel loaded PLGA: Poloxamer blend nanoparticles for cancer chemotherapy. *International journal of biological macromolecules, 69*, 393–399.
79. Kim, D., El-Shall, H., Dennis, D., & Morey, T. (2005). Interaction of PLGA nanoparticles with human blood constituents. *Colloids and Surfaces B: Biointerfaces, 40*, 83–91.
80. Shalini, V., & Srinivas, L. (1987). Lipid peroxide induced DNA damage: Protection by turmeric (Curcuma longa). *Molecular and cellular biochemistry, 77*, 3–10.
81. Haider, K., Haider, M. R., Neha, K., & Yar, M. S. (2020). Free radical scavengers: An overview on heterocyclic advances and medicinal prospects. *European Journal of Medicinal Chemistry, 204*, 112607.
82. Demir, Y., Taslimi, P., Koçyiğit, Ü. M., Akkuş, M., Özaslan, M. S., Duran, H. E., Budak, Y., Tüzün, B., Gürdere, M. B., & Ceylan, M. (2020). Determination of the inhibition profiles of pyrazolyl–thiazole derivatives against aldose reductase and α-glycosidase and molecular docking studies. *Archiv der pharmazie, 353*, 2000118.
83. Khalifa, N., Nossier, E., & Al-Omar, M. (2017). Synthesis and characterization of new pyrazolyl-substituted thiazolidinone, thiazole, and thiazoline candidates. *Russian Journal of General Chemistry, 87*, 1295–1299.
84. Alfi, A. A., Alharbi, A., Qurban, J., Abualnaja, M. M., Abumelha, H. M., Saad, F. A., & El-Metwaly, N. M. (2022). Molecular modeling and docking studies of new antioxidant pyrazole-thiazole hybrids. *Journal of Molecular Structure, 1267*, 133582.

85. Shih, M.-H., Su, Y.-S., & Wu, C.-L. (2007). Syntheses of aromatic substituted hydrazino-thiazole derivatives to clarify structural characterization and antioxidant activity between 3-arylsydnonyl and aryl substituted hydrazino-thiazoles. *Chemical and Pharmaceutical Bulletin, 55*, 1126–1135.